

Electronic Supplementary Information (ESI):

Ultra-Low Overpotential and High Rate Capability in Li-O₂ Batteries through Surface Atom Arrangement of PdCu Nanocatalysts

Ran Choi,^{a,‡} Jaepyeong Jung,^{b,‡} Gyubong Kim,^c Kyeongse Song,^b Yong-Il Kim,^d Sung Chul Jung,^b Young-Kyu Han,^{b,*} Hyunjoon Song^{a,*} and Yong-Mook Kang^{b,*}

^a Department of Chemistry, Korea Advanced Institute of Science and Technology(KAIST); Center for Nanomaterials and Chemical Reactions, Institute for Basic Science (IBS), Daejeon, 305-701, Korea

E-mail: hsong@kaist.ac.kr

^b Department of Energy and Materials Engineering, Dongguk University-Seoul, Seoul, 100-715, Korea

E-mail: ykenery@dongguk.edu, dake1234@dongguk.edu

^c Division of Materials Science, Korea Basic Science Institute (KBSI), Daejeon, 305-333, Korea

^d Korea Research Institute of Standards and Science (KRISS), Daejeon, 305-340, Korea

Experimental Section

Chemicals and Materials. Na_2PdCl_4 (98%), $\text{Cu}(\text{C}_2\text{H}_2\text{O}_4)$ (97%), PVP ($M_w \approx 55,000$), EG ($\geq 99\%$), and benzyl amine (99%) were purchased from Aldrich and used without further purification.

Synthesis of PdCu NPs. All reactions were carried out under an Ar atmosphere. Na_2PdCl_4 (50 mg) was mixed with poly(vinyl pyrrolidone) (PVP, 190 mg) in ethylene glycol (EG, 10 mL), and $\text{Cu}(\text{C}_2\text{H}_2\text{O}_4)$ (52 mg) was separately dissolved in benzyl amine (0.5 mL). The solutions were mixed with vigorous stirring. The molar ratio of the repeating unit of PVP ($M_w = 111$) to the Pd precursor was 10:1. The solution was heated at 200 °C for 1 h. During the reaction, the solution color turned from bluish green to orange and eventually black-brown. The reaction mixture was cooled down to room temperature. Acetone (20 mL) was added to the mixture to precipitate the particles with the aid of centrifugation (4500 rpm, 30 min). The resulting PdCu NPs were thoroughly washed with ethanol and acetone.

Synthesis of Pd NPs. Na_2PdCl_4 (100 mg) and PVP (95 mg) were dissolved in EG (13 mL) with vigorous stirring. The molar ratio of the repeating unit of PVP to the Pd precursor was 2.5:1. The solution was heated at 200 °C for 3 h. During the reaction, the solution color turned from orange to black-brown. The reaction mixture was cooled down to room temperature. Acetone (10 mL) and toluene (20 mL) were added into the mixture to precipitate the particles with the aid of centrifugation (4500 rpm, 30 min). The resulting Pd NPs were thoroughly washed with ethanol, acetone, and toluene.

Characterization of NPs. TEM images were obtained with an Omega EM912 energy-filtering transmission electron microscope (EF-TEM, Carl Zeiss) operated at 120 kV. HRTEM images were taken using a Tecnai G2 F30 field-emission transmission electron microscope (FE-TEM, FEI Company) operated at 300 kV. SEM images were obtained with a field emission scanning electron microscope (FE-SEM; JEOL JSM-6700F, operated at 10 and 30 kV). The composition of the PdCu NPs was determined by ICP-AES (OPTIMA 7300 DV, Perkin-Elmer). XPS measurements were carried out using a Thermo MultiLab 2000 spectrometer with Al $K\alpha$ X-ray (1486.6 eV) as the light source. X-ray diffraction data were collected over the scattering angle range $20^\circ \leq 2\theta \leq 125^\circ$ at a 2θ step of 0.02° using $\text{Cu}K_\alpha$ radiations with a graphite monochromator in the reflection geometry at 298 K (Rigaku, Dmax2200). The EXPGUI program, which is a graphical user interface for the General Structure Analysis System (GSAS), was used to perform the Rietveld refinement.^{1,2} The pseudo-Voigt function was used as a profile function.³

Electrochemical Measurements. To make the electrode, the active material, Ketjen black (EC600JD) and a PVDF-HFP copolymer with a weight ratio of 40:45:15 were mixed in N-methylpyrrolidone (NMP) as a solvent. The resulting slurries were pasted onto a carbon paper (GDL;

gas diffusion layer) and then dried in a vacuum oven at 120 °C for 5 h. The carbon weight and metal NPs catalysts weight in the electrode was 0.27 mg and 0.24 mg, respectively. In addition, the metal NPs catalysts on electrode had average loading density of 0.21 mg cm⁻² and average loading weight of 0.24 mg. The Swagelok-type cell was assembled with the electrode, a Li metal foil as a counter electrode, a glass fiber (0.7 μm pore size) as a separator, and 1 M of LiCF₃SO₃ dissolved in tetra(ethylene glycol) dimethyl ether (TEGDME) as a electrolyte in an Ar-filled glove box (<1 ppm H₂O). Subsequently, the sealed cells were purged with O₂ gas (purity, 99.995%) for 10 min and closed after the pressure reached 1.1 atm. The cell was galvanostatically charged and discharged at 200 mA g_{carbon}⁻¹. For the stabilization of cycling, the cell was also tested using a constant current – constant voltage (CC – CV) mode with potentiostatic steps at 4.2 V under limited capacity condition (1000 mAh g_{carbon}⁻¹). The various rates ranging from 200 to 5000 mA g_{carbon}⁻¹ with a low voltage limit of 2.0 V were measured.

Computational Details. First-principles calculations were performed using the density functional theory (DFT) with the projector augmented wave pseudo potentials as implemented in the Vienna *Ab initio* Simulation Package (VASP).^{4,5} The electron exchange-correlation was treated within the spin-polarized generalized gradient approximation of the Perdew–Burke–Ernzerhof type.⁶ The cutoff energy for the plane wave-basis expansion was chosen to be 400 eV and the atomic relaxation was continued until Hellmann–Feynman forces acting on atoms were less than 0.02 eV Å⁻¹. Adsorption/desorption of Li_xO₂ ($x = 1, 2, \text{ and } 4$) clusters on the Pd, Cu, and PdCu alloy surfaces were calculated as the intermediates of ORR and OER processes as addressed in the literatures.⁷⁻⁹ The intermediates of Li_xO₂ on Pd(111) and Cu(111) were calculated with the 3×3 unit cell of these surfaces. For the PdCu alloy systems, we employed the *B2-type* structure that is known as the ordered phase of the PdCu alloy.¹⁰ The PdCu(111), (110) and (100) surfaces were used with the unit cell sizes of 2×2, 2×3 and 3×3, respectively. All simulated metal surfaces were modeled by the slabs of four atomic layers separated by 13 Å of vacuum. The bottommost layers were fixed to maintain their bulk atomic distances during the structure relaxation, where the distances are 2.80, 2.57 and 2.61 Å for Pd, Cu, and PdCu, respectively, obtained from our calculations. The Brillouin zone was sampled using Γ -centered 5×5×1 *k*-point mesh and the electronic states were smeared using the Methfessel-Paxton scheme with a broadening width of 0.1 eV.

The average energy of the surface *d* electrons, termed *d*-band center, has been widely accepted as one possible measure of the reactivity of metal catalyst surfaces.^{11,12} However, the *d*-band center model should be applied carefully to the systems with similar *d*-band filling and charge states.^{13,14} We found that the *d*-band center is rarely correlated to the binding energies of LiO₂ on the Pd, Cu, and PdCu surfaces, thus direct calculations of overpotentials are necessary to understand the ORR and OER of these surfaces. The overpotentials (η) of ORR and OER were calculated as $\eta_{\text{ORR}} = U_0 - U_{\text{DC}}$ and $\eta_{\text{OER}} = U_{\text{C}} - U_0$, where U_0 , U_{DC} and U_{C} are equilibrium, discharging and charging potentials, respectively, and were included in Table 1 for all the calculated metal surfaces. U_{DC} was

determined by the value of U at which the reaction energies of all intermediate steps are positive, while U_C is the lowest potential where charging is downhill except the $\text{Li}_2\text{O bulk} \rightarrow (\text{Li}_2\text{O})_2^*$ step involve no electron (Li ion) transfer, thus is not affected by the applied potential U . Such calculation procedure of η in theory was employed in the previous studies.^{8,9,15,16}

Table S1 Refined structural parameters of PdCu alloys obtained from the Rietveld refinement using X-ray powder diffraction data at 297 K. The symbol, *g*, is the occupation factor. The numbers in parentheses are the estimated standard deviations of the last significant figure.

FCC						
Atom	Site	<i>x/a</i>	<i>y/b</i>	<i>z/c</i>	<i>g</i>	<i>B_{eq}/Å²</i>
Cu(1)	4 <i>a</i>	0.0	0.0	0.0	0.5178(2) ¹⁾	0.023(2) ²⁾
Pd(1)	4 <i>a</i>	0.0	0.0	0.0	0.4822(2)	0.023(2)

Space group : *Fm-3m* (No. 225) and *Z* = 1
a = *b* = *c* = 3.7675(7) Å

B2-type						
Atom	Site	<i>x/a</i>	<i>y/b</i>	<i>z/c</i>	<i>g</i>	<i>B_{eq}/Å²</i>
Cu(2)	1 <i>a</i>	0.0	0.0	0.0	1.0	0.043(2)
Pd(2)	1 <i>b</i>	1/2	1/2	1/2	1.0	0.021(2)

Space group : *Pm-3m* (No. 221) and *Z* = 1
a = *b* = *c* = 2.9892(6) Å

Weight fraction	
FCC	B2-type
48.95(1) %	51.05(1) %

1) Constraint on occupancy: $g[\text{Cu}(1)] + g[\text{Pd}(1)] = 1.0$.

2) Constraint on isotropic atomic displacement: $B_{\text{eq}}[\text{Cu}(1)] = B_{\text{eq}}[\text{Pd}(1)]$.

R-factor

$R_{\text{wp}} = 2.43$, $R_{\text{p}} = 1.87$, $R_{\text{e}} = 1.63$ and $S (= R_{\text{wp}}/R_{\text{e}}) = 1.49$

Table S2 Pd/Cu weight and atomic percent of PdCu NPs, synthesized in the absence of benzyl amine, determined by EDS.

Element	Weight %	Atomic %
CuK	5.17	8.37
PdK	94.82	91.62

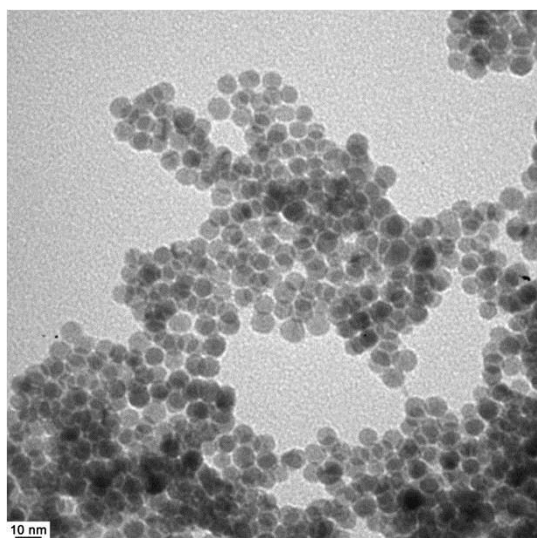


Fig. S1 TEM image of PdCu NPs with size of 7.8 ± 0.8 nm.

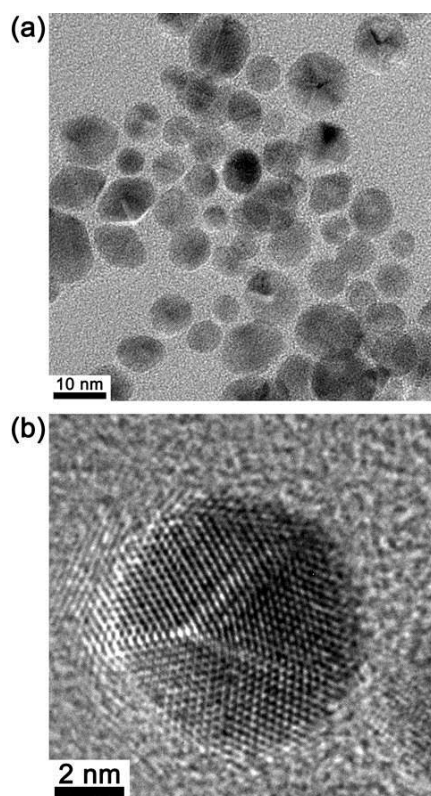


Fig. S2 (a) TEM and (b) HRTEM images of PdCu NPs synthesized without benzyl amine under the present conditions. The HRTEM image indicates polycrystalline nature of the PdCu NPs with grain boundaries, which are mainly caused by the slow reduction rate of Cu element.

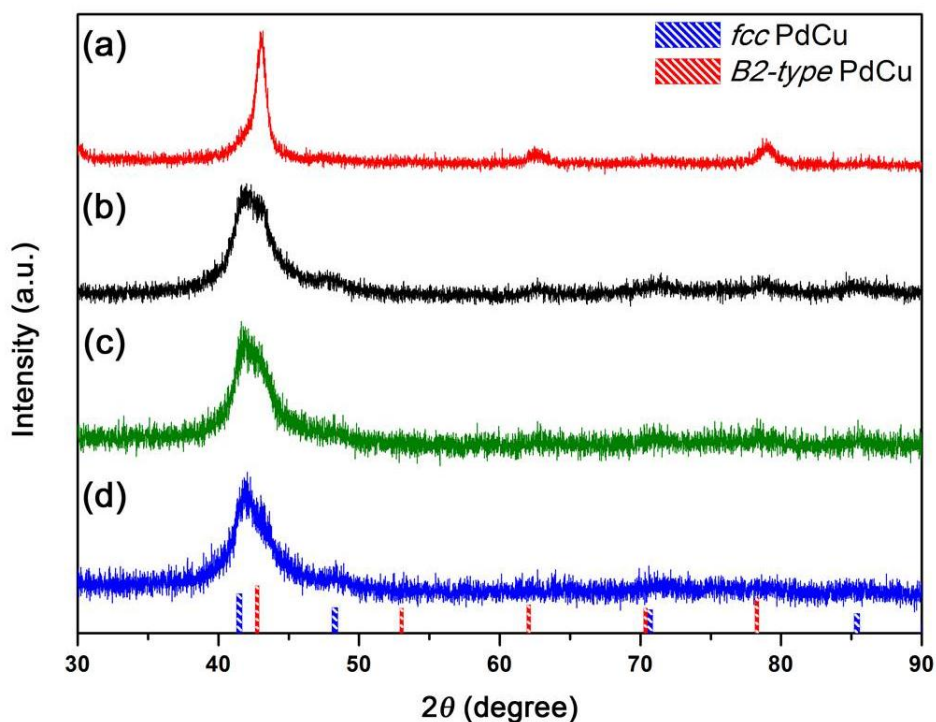


Fig. S3 The XRD patterns of PdCu NPs depending on the amount of benzyl amine during synthesis. The XRD patterns of PdCu NPs prepared by 1 h heating as the added volumes of benzyl amine are (a) 1.0 mL, (b) 0.50 mL, and (c) 0.25 mL, respectively. (d) The XRD pattern of PdCu NPs synthesized by 0.5 h heating when the added volume of benzyl amine is 0.25 mL.

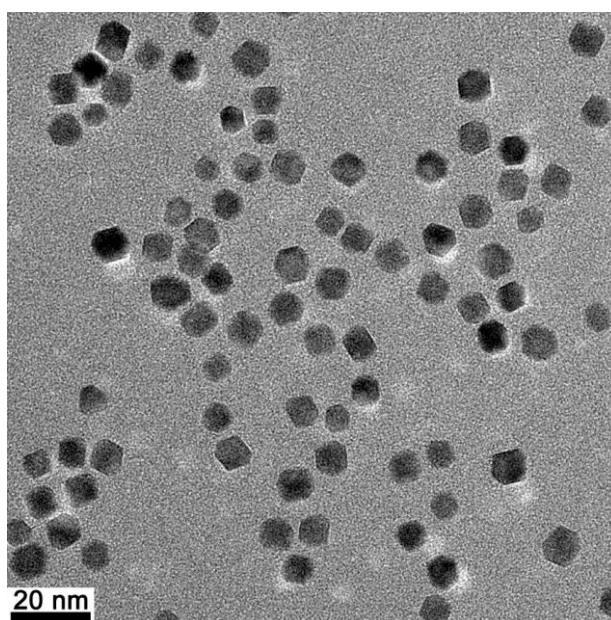


Fig. S4 TEM image of Pd NPs synthesized by a polyol method. The Pd NPs have the average size of 7.8 ± 0.7 nm, which is identical to that of the PdCu NPs.

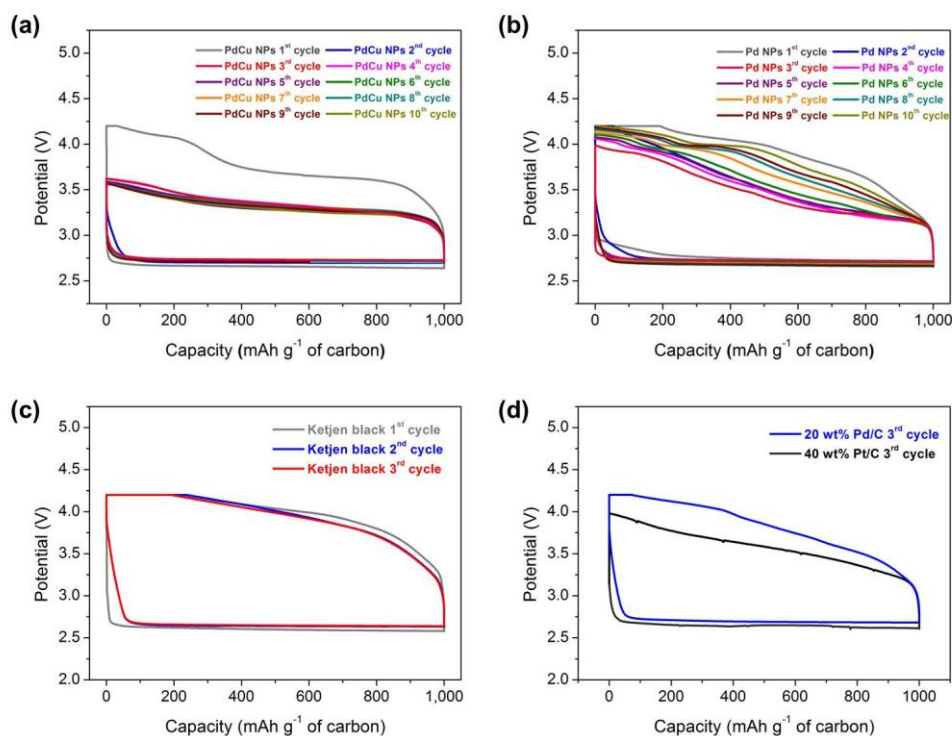


Fig. S5 The discharge/charge voltage profiles during the initial ten cycles for (a) PdCu, (b) Pd NPs and (c) The discharge/charge voltage profiles during the initial three cycles for Ketjen black at the current density of 200 mA g_{carbon}⁻¹. (d) The third galvanostatic discharge/charge voltage profiles of commercial Pd/C and Pt/C catalysts.

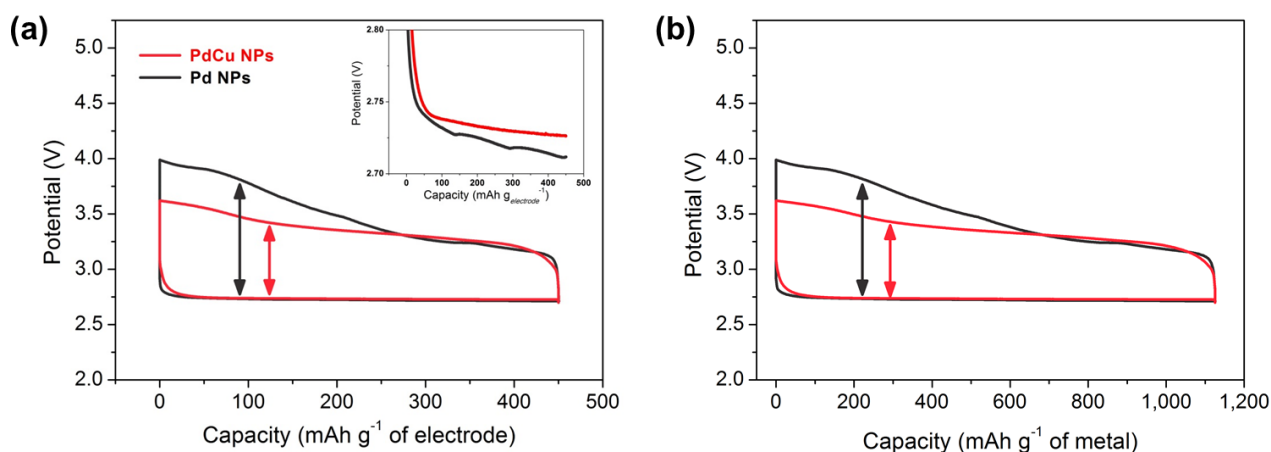


Fig. S6 The third galvanostatic discharge/charge voltage profiles normalized by the weight of (a) electrodes (0.6 mg) and (b) the weight of metal catalysts (0.24 mg for PdCu, 0.21 mg cm⁻²) for PdCu and Pd NPs.

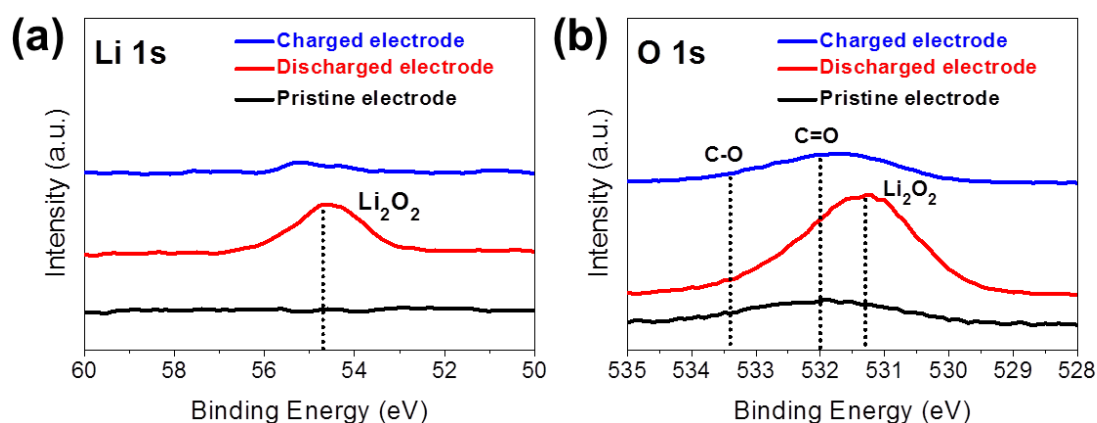


Fig. S7 XPS spectra of a cathode with PdCu catalysts during cycling; (a) Li 1s partial spectra, (b) O 1s partial spectra of the pristine, discharged and charged cathodes. Li 1s and O 1s binding energies of the discharged cathode well agree with the Li 1s (54.7 eV) and O 1s (531.3 eV) binding energies of Li_2O_2 .¹⁷ The 1s spectra of Li and O for charged electrode prove that the discharge products (Li_2O_2) can be completely decomposed.

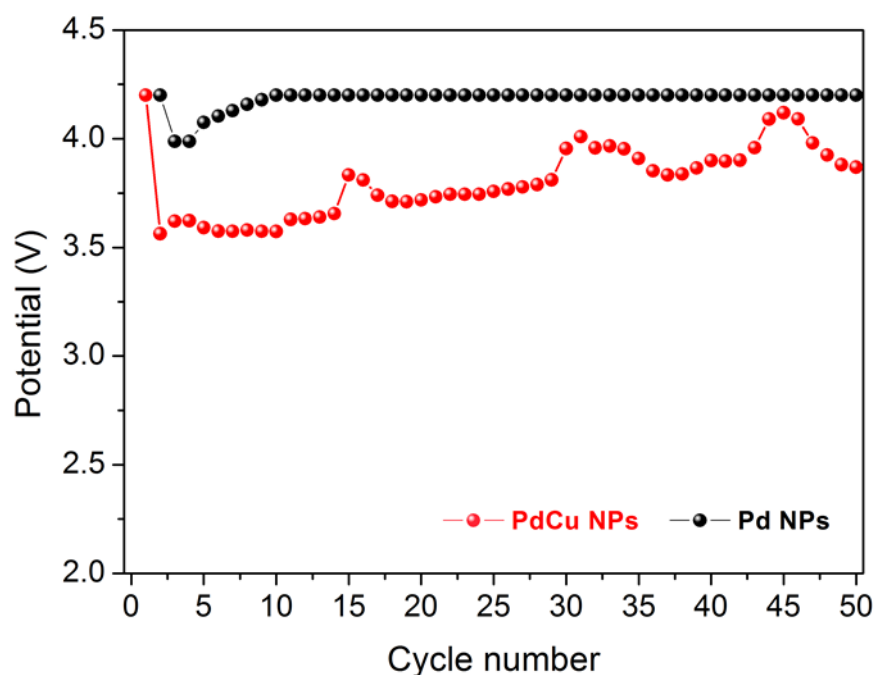


Fig. S8 The cyclic behaviors of OER end-potentials measured at the current density of 200 mA $\text{g}_{\text{carbon}}^{-1}$

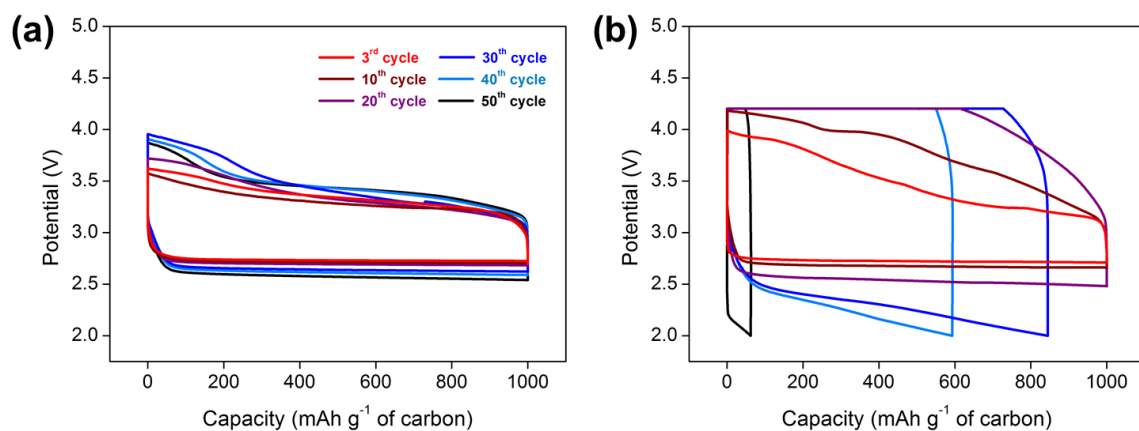


Fig. S9 The galvanostatic discharge/charge profiles of (a) the PdCu catalyst and (b) the Pd catalyst after the 3rd, 10th, 20th, 30th, 40th and 50th cycle.

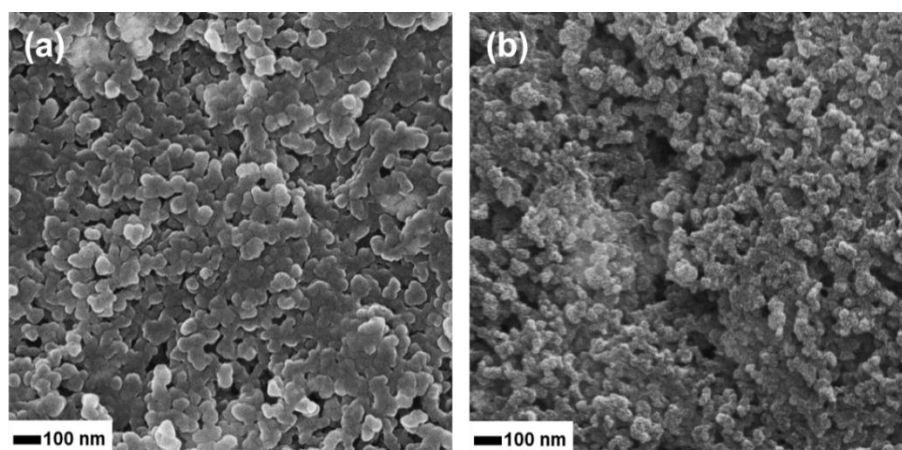


Fig. S10 SEM images of (a) pristine cathode, and (b) the charged cathode at 50th cycle, adopting PdCu NPs as the cathode catalyst.

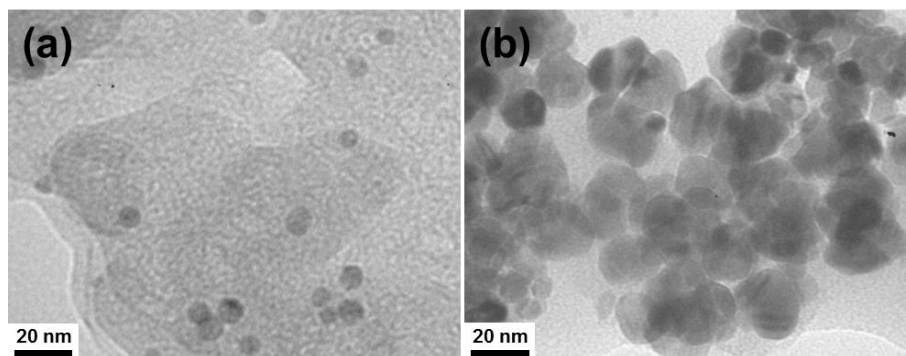


Fig. S11 TEM images of (a) PdCu and (b) Pd NPs after 50 cycles.

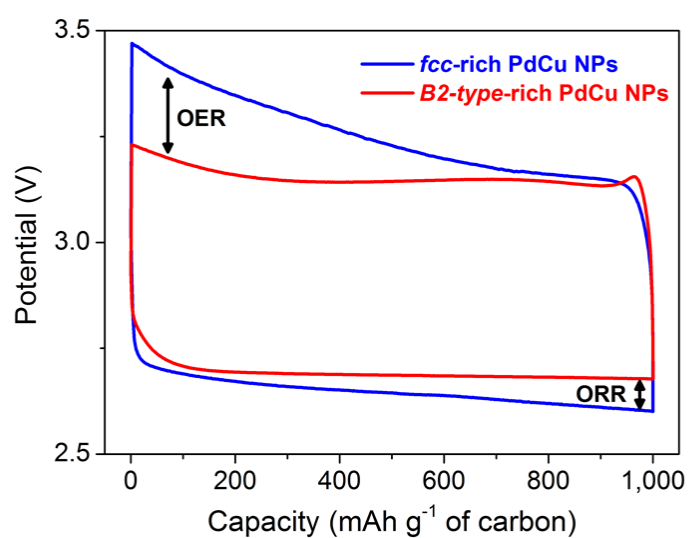
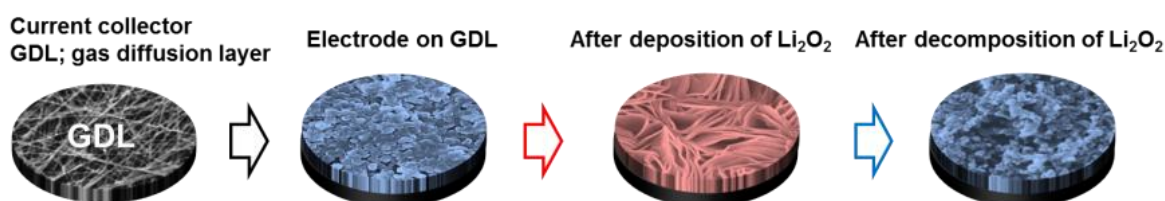


Fig. S12 The galvanostatic discharge/charge profiles of *fcc*-rich (blue line) and *B2-type*-rich (red line) PdCu NPs at the current density of $200 \text{ mA g}_{\text{carbon}}^{-1}$.



Discharge capacity calculation using above the actual mass of deposited Li_2O_2 via following equation :

$$\text{weight of } \text{Li}_2\text{O}_2 \text{ (g)} = \frac{MW_{\text{Li}_2\text{O}_2} \cdot \text{discharge capacity (C)}}{n \cdot F \text{ (C/mol)}}$$

where $MW_{\text{Li}_2\text{O}_2}$ is the molecular weight of Li_2O_2 (45.882 g/mol), n is the number of electron transferred of the discharge reaction assuming final product as Li_2O_2 ($n = 2$), F is Faraday constant (96485 C/mol).

Fig. S13 Specific capacity normalization method using the weight of discharge product (Li_2O_2).¹⁸

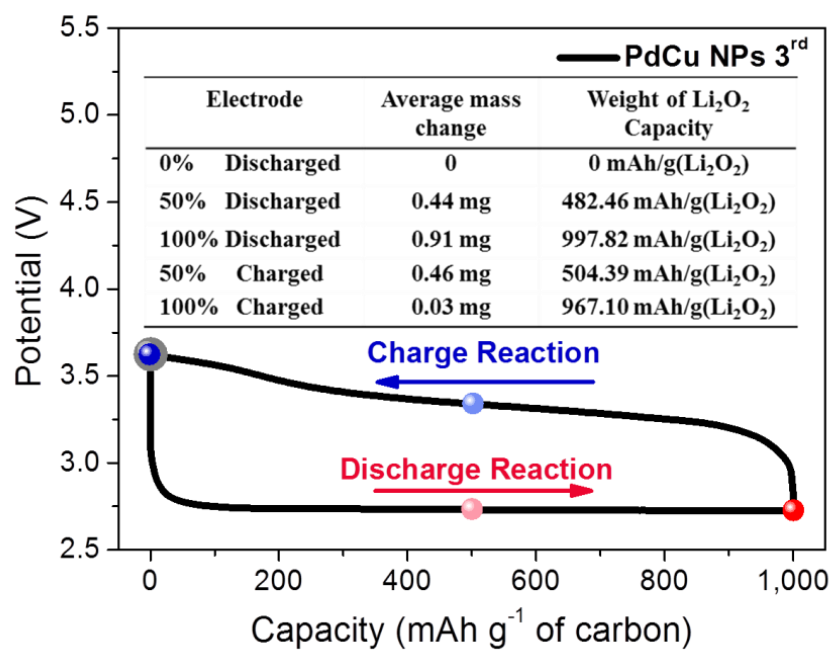


Fig. S14 The mass change variation of PdCu NPs electrode during 3rd cycle; gray-colored point corresponds to pristine electrode and red-colored point indicates the discharged state (Li₂O₂ formation), whereas blue-colored point corresponds to the charged state (Li₂O₂ dissociation).

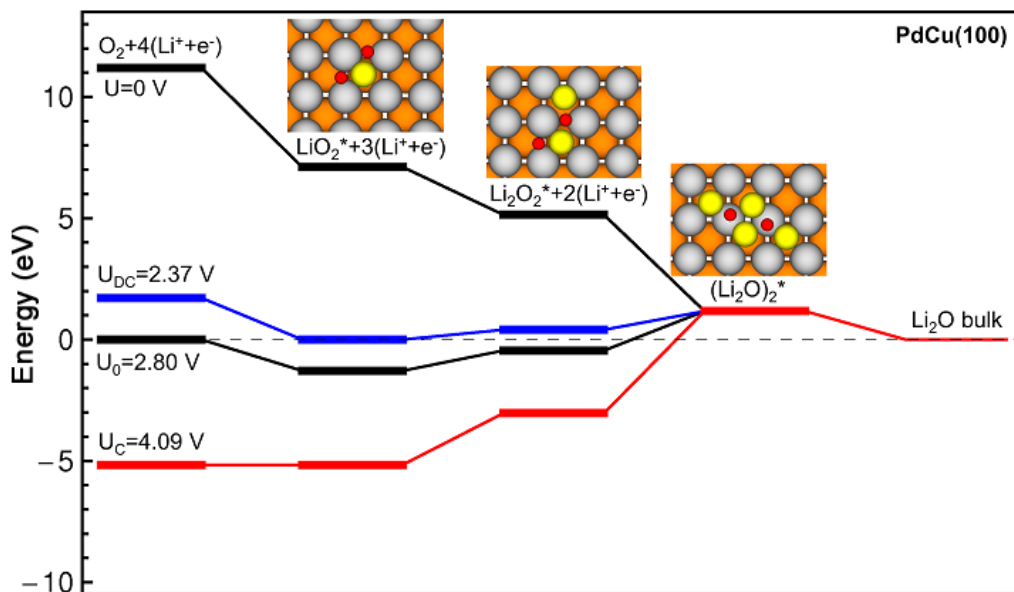


Fig. S15 Energy diagrams of ORR and OER on PdCu(100) with the optimized geometries of Li_xO_2 adsorption. The gray, orange, red, and yellow balls denote the Pd, Cu, O, and Li atoms, respectively.

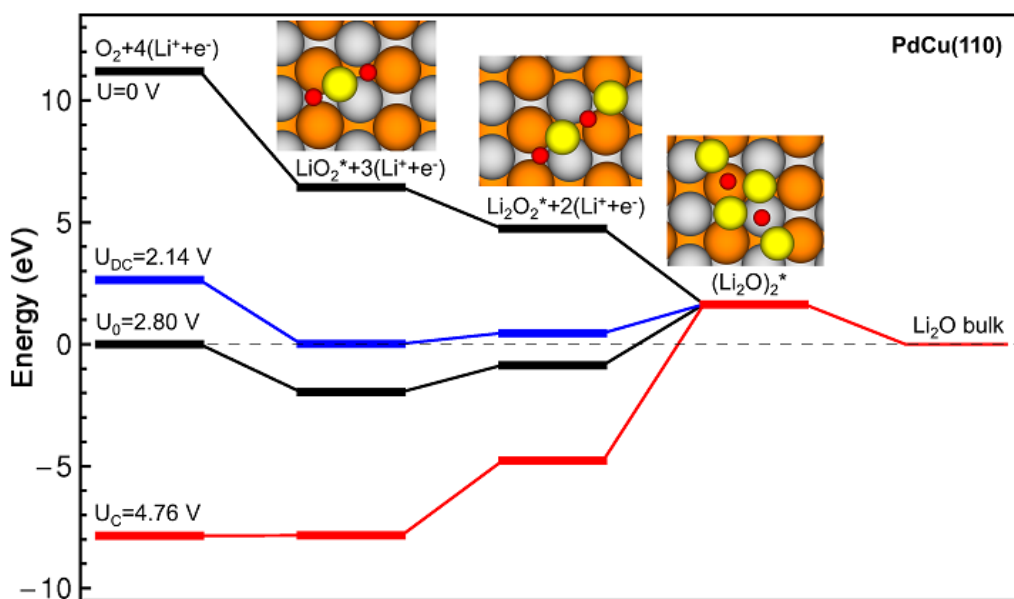


Fig. S16 Energy diagrams of ORR and OER on PdCu(110) with the optimized geometries of Li_xO_2 adsorption. The gray, orange, red, and yellow balls denote the Pd, Cu, O, and Li atoms, respectively.

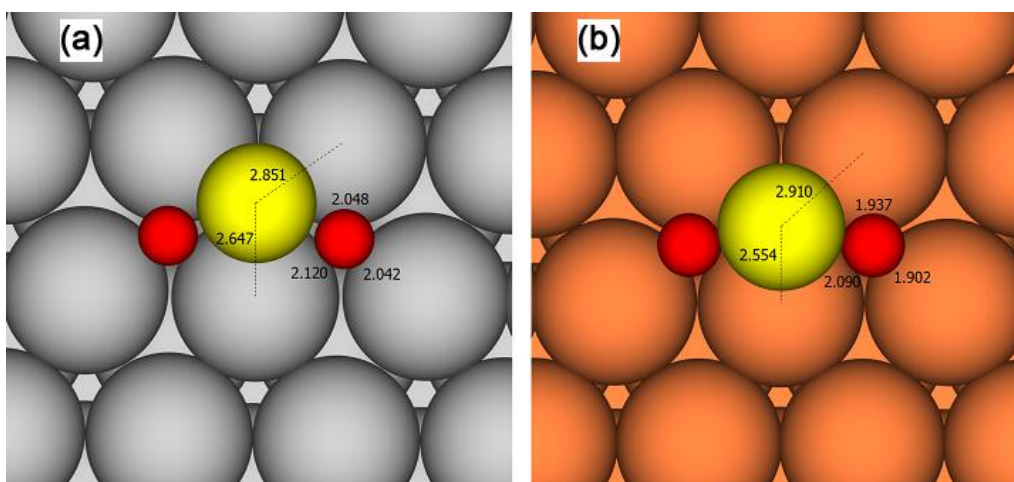


Fig. S17 Optimized geometries of LiO_2 adsorption on (a) Pd(111) and (b) Cu(111) with the binding distances, r (Å), from the metal atoms to Li and O atoms. The gray, orange, red, and yellow balls denote the Pd, Cu, O, and Li atoms, respectively.

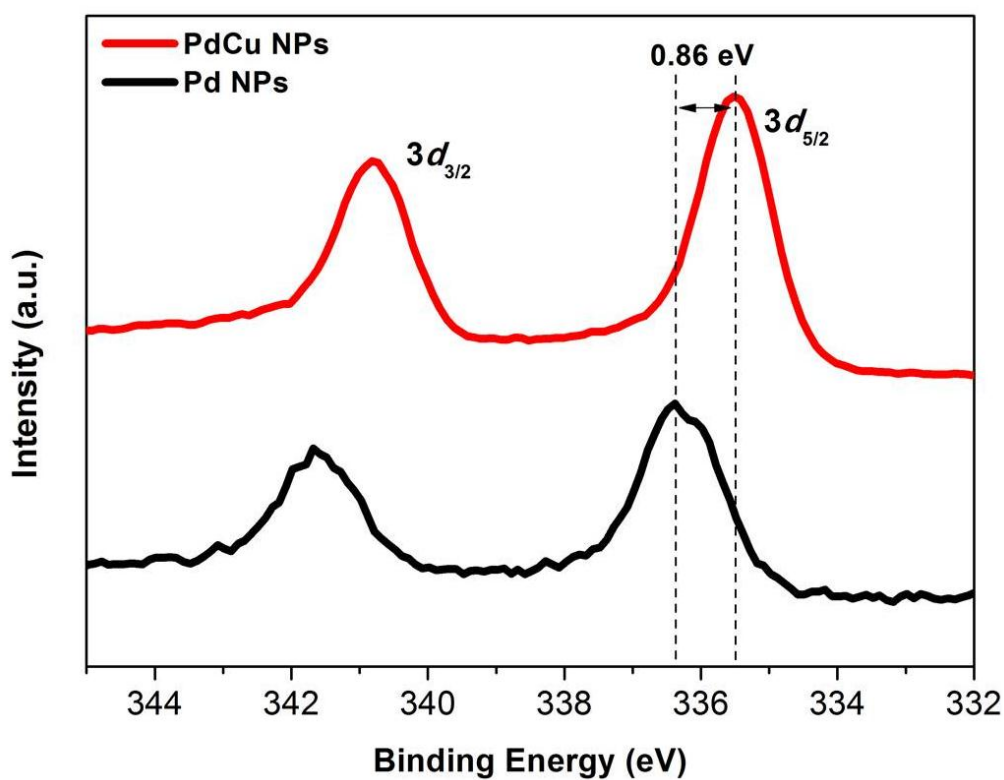


Fig. S18 XPS spectra of the Pd 3d core level of PdCu (red) and Pd (black) NPs.

References

- 1 B. H. Toby, *EXPGUI*, *J. Appl. Cryst.*, 2001, **34**, 210-213.
- 2 A. C. Larson, R. B. Von Dreele, *Los Alamos National Laboratory Report LAUR*, 1994, 86-748.
- 3 P. Thompson, D. E. Cox, J. B. Hastings, *J. Appl. Cryst.*, 1987, **20**, 79-83.
- 4 G. Kresse, J. Furthmüller, *Phys. Rev. B*, 1996, **54**, 11169-11186.
- 5 G. Kresse, D. Joubert, *Phys. Rev. B*, 1999, **59**, 1758-1775.
- 6 J. P. Perdew, K. Burke, M. Ernzerhof, *Phys. Rev. Lett.*, 1996, **77**, 3865-3868.
- 7 Y. Xu, W. A. Shelton, *J. Chem. Phys.*, 2010, **133**, 024703(1)-024703(9).
- 8 G. K. P. Dathar, W. A. Shelton, Y. Xu, *J. Phys. Chem. Lett.*, 2012, **3**, 891-895.
- 9 J. S. Hummelshøj, J. Blomqvist, S. Datta, T. Vegge, J. Rossmeisl, K. S. Thygesen, A. C. Luntz, K. W. Jacobsen, J. K. Nørskov, *J. Chem. Phys.*, 2010, **132**, 071101(1)-071101(4).
- 10 N. Lopez, J. K. Nørskov, *Surface Science*, 2001, **477**, 59-75.
- 11 J. K. Nørskov, T. Bligaard, J. Rossmeisl, C. H. Christensen, *Nat. Chem.*, 2009, **1**, 37-46.
- 12 G. Kim, Y. Kawazoe, K.-R. Lee, *J. Phys. Chem. Lett.*, 2012, **3**, 1989-1996.
- 13 B. Hammer, J. K. Nørskov, *Adv. Catal.*, 2000, **45**, 71-129.
- 14 J. R. Kitchin, J. K. Nørskov, M. A. Barteau, J. G. Chen, *J. Chem. Phys.*, 2004, **120**, 10240-10246.
- 15 Y. Mo, S. P. Ong, G. Ceder, *Phys. Rev. B*, 2011, **84**, 205446(1)-205446(9).
- 16 J. K. Nørskov, J. Rossmeisl, A. Logadottir, L. Lindqvist, *J. Phys. Chem. B*, 2004, **108**, 17886-17892.
- 17 Y. C. Lu, E. J. Crumlin, G. M. Veith, J. R. Harding, E. Mutoro, L. Baggetto, N. J. Dudeny, Z. Liu, Y. Shao-Horn, *Sci. Rep.* 2012, **2**, 715-720
- 18 J. Jung, K. Song, D. R. Bae, S. W. Lee, G. Lee, Y.-M. Kang, *Nanoscale*, 2013, **5**, 11845-11849.